Journal of Materials Chemistry A

Accepted Manuscript

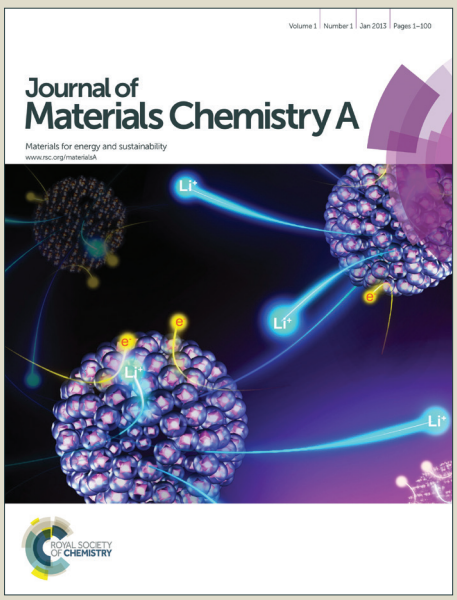

ROYAL SOCIETY OF CHEMISTRY

www.rsc.org/materialsA

Journal of Materials Chemistry A

ARTICLE

A three layer design with mesoporous silica encapsulated by carbon core and shell for high energy Lithium ion battery anode

Xi Cao[a,b], Xiuyun Chuan[*a], Robert Masse[b], Dubin Huang[a], Shuang Li[b], Guozhong Cao[*b]

Received 00th January 20xx,
Accepted 00th January 20xx

DOI: 10.1039/x0xx00000x

www.rsc.org/MaterialsA

Novel C/SiO_2 composite with a carbon-silica-carbon (C-mcms) three layer structure was synthesized and evaluated as an anode material for high-energy lithium ion batteries. The C-mcms exhibits excellent capacity of about 1055 mAh·g^{-1} at a current density of 500 mA·g^{-1} after 150 cycles without detectable decay, and high-rate capability, which is superior to other similar composites without the carbon core or the carbon shell. The results indicate the structural effect on the enhancement of the electrochemical properties: the SiO_2 nanoparticles are completely confined between the carbon shell and the carbon core, the two carbon parts work together to keep the structural integrity and to keep the electrode to be highly conductive and active during cycling, which guarantees the high capacity and cycle stability; the interior pores and voids among the SiO_2 nanoparticles can provide free space to accommodate the volume change and buffer the volume effect of the electrode during lithiation/delithiation.

1. Introduction

As one of the most important candidates for the power source of portable electric devices, electric vehicles (EVs) and hybrid electric vehicles (HEVs), lithium ion batteries (LIBs) are attracting great interest due to their high energy density, long cycling life, and environmental friendliness. There is an increasing demand for rechargeable lithium-ion batteries with higher energy density and longer cycle life for applications to meet the rapid development in large-scale energy applications[1-5]. Carbonaceous material is commercially used as an anode material due to its advantages of long cycle life, relatively safety and low cost. However, its low lithium-storage capacity (LiC_6: 372 mAh·g^{-1}) cannot satisfy the continuously increasing requirement nowadays. Various efforts have been made to developing new and better electrode materials with higher specific capacity and tailoring materials to new nanostructures in order to enhance their electrochemical performance [4, 6-10]. Silicon based materials have attracted great interest due to the significantly higher theoretical specific capacity of about 4200 mAh·g^{-1} for $Li_{22}Si_5$ alloy, low-cost and higher safety. However, the severe volume change (>300%) occurring during lithium insertion/extraction process leads to active particle cracking, electrode pulverization, and subsequent loss of electrical contact between active material and current collector, resulting in severe capacity degradation. Several strategies have been proposed to deal with this problem, including the preparation of nanostructured Si [11-15] and composite materials [16-21]. By dispersing nano-Si particles in carbon matrix, the electrochemical performance could be improved significantly. However, complex strategies are often required to prepare the refined nanostructures, and the high cost of nano silicon makes the anode composite far from industrial application level.

As a replacement, although having a specific capacity lower than that of Si (with the largest reversible capacity of 1961 $mAhg^{-1}$; the theoretical capacity of SiO_2 can be calculated according to different types of reactions exist between silica and lithium ions proposed in previous study, detailed mechanism and calculation is listed in the supporting information[22-25]), SiO_2 has also received a lot of interest due to its extremely low cost, less volume change during cycling. Even though lithium oxides and lithium silicates generated in the first discharge process act as buffer layers to accommodate the volume change of the amorphous Si particles to some extent [24-28], however, the volume effect, along with low initial coulombic efficiency and poor electrical conductivity still remains to be the main obstacles to enhance the electrochemical performance. A lot of efforts have been done to address these problems, such as synthesizing silica materials with carbon coating and different nanostructures. For example, Chang et al.[23] reported that a 24 h high energy mechanical milled SiO_2 would generate 5 nm Si crystallites dispersed randomly within the amorphous silicon and exhibit a reversible capacity of ~800 mAh·g^{-1} at a current of 100 mA·g^{-1} over 100 cycles. Amorphous SiO_2/C composite prepared by mechanical milling and post heat-treatment exhibited high reversible capacity of 600 mAh·g^{-1} [29]. Hollow porous SiO_2 nanocubes, hollow silica nanospheres and SiO_2 nanotubes were also synthesized by a sacrificial template method and studied as anode materials [22, 28, 30]. However, these methods may encounter time-consuming, environmental pollution and other issues. Thus, preparing SiO_2 based composites with controllable nanostructure and high capacity in a facile method is required to the actual application.

In this work, a new type of C/SiO_2 composite with a carbon-silica-carbon three layer structure was prepared in a facile method, with mesoporous silica encapsulated by the carbon

[a] School of Earth and Space Science, Peking University, Beijing 100871, PR China. E-mail: xychuan@pku.edu.cn. Tel: 86-10-62767965. Fax: 86-10-62751159.
[b] Department of Materials Science and Engineering, University of Washington, Seattle, Washington 98195, USA. E-mail: gzcao@u.washington.edu. Tel.: +1-206-616-9084. Fax: +1-206-543-3100.

core and shell. When studied as an anode material in lithium ion batteries, this composite exhibits an excellent electrochemical performance with a high specific capacitance, good cycling performance and excellent rate capability. The significant impacts of the carbon core and carbon shell in enhancing the performance were systematically investigated.

2. Experimental

2.1Synthesis

The fabrication of C/SiO_2 composite with a carbon-silica-carbon three layer structure is illustrated in Fig. 1. Firstly, monodispersed mesoporous polymer nanospheres were prepared by a low-concentration hydrothermal method according to the literature[31]. Secondly, 0.2g synthesized mesoporous polymer nanospheres was added into a solution containing 100 ml of H_2O, 60 ml of ethanol and 300 mg of cetyltrimethyl ammonium bromide (CTAB) and dispersed in an ultrasonication bath for 30 min. Then 1.65 ml of ammonia (28 wt %) was added into the mixture with mechanical stirring for another 30 min. 0.5 ml of tetraethyl orthosilicate (TEOS) was added into the above solution every 30 minutes and totally 3 times, then the mixture was stirred for 12 h. The assembled cationic surfactant micelle templates(CTAB) serves as structure-directing agents for polymerizing silica component by electrostatic interaction. After the product was collected by centrifugation and washed with H_2O and ethanol for three times, respectively, the CTAB should be removed, then, after calcined under an Ar flow at 500 ℃ for 3 h at a heating rate of 3 ℃/min, the uniform core/shell mesoporous carbon-mesoporous silica (denoted as mcms) was obtained. Finally, 0.2 g obtained mcms was dispersed in a solution containing 10 ml of H_2O, 10 ml of ethanol and 0.5 g of sucrose, then transferred into a 30 ml polytetrafluoroethylene (PTFE)-lined stainless steel autoclave and kept at 120℃ for 4 h. The precipitate was collected and washed several times by centrifugation with deionized water after the autoclave was cooled down, then dried at 80 ℃ overnight. The composites were annealed at 800 ℃ for 3 h under Ar flow to form the carbon-silica-carbon three layer structured composites (C-mcms).

In comparison, carbon core-mesoporous silica shell nanospheres without carbon coated on the surface (denoted as mcms) and the carbon coated hollow silica nanospheres (without carbon core, denoted as C-ms) were also studied, as shown in Fig. 2.

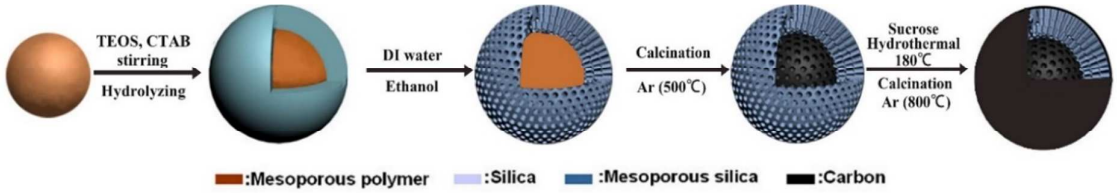

Fig. 1 Preparation of the carbon -silica-carbon three layer structure C/SiO_2 composite.

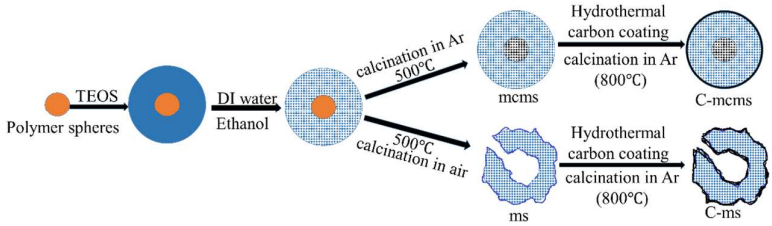

Fig.2 Preparation procedure of the mcms, C-mcms and C-ms composites.

2.2Structural analyses

The crystal structure of the obtained sample was characterized by means of X-ray diffraction (XRD, D8 Bruker X-ray diffractometer with Cu-Ka radiation (λ=1.5418Å) within the range of 10-80° (2θ). The morphology was examined using scanning electron microscopy (SEM, JEOL JSM-7000F). Transmission electron microscopy (TEM) measurements were conducted on a Tecnai F20 microscope (FEI) operating at 200 kV accelerating voltage. The samples were suspended in ethanol and transferred onto a Cu grid for TEM measurements. The content of SiO_2 was determined from the mass loss of the samples at 800 ℃ in air with a Q50 thermo gravimetric (TGA) apparatus (TA, USA).

Nitrogen adsorption-desorption isotherms were measured using Quantachrome NOVA 4200e system. Samples were degassed at 200℃ for 10 h under vacuum prior to measurements. The specific surface area and pore size distribution were determined by multipoint Brunauer-Emmett-Teller (BET), Density functional theory (DFT) desorption analyses, respectively.

X-ray photoelectron spectroscopy (XPS) analysis was performed using a Surface Science Instruments S-probe spectrometer with a monochromatized Al Ka X-ray and a low-energy electron flood gun for charge neutralization. The accelerating voltage and current were 40 kV and 40 mA, respectively. Three spots were tested on each sample to make final results credible.

2.3Electrochemical measurements

The electrochemical performance was tested in sandwich-type two-electrode coin cells. In order to prepare the working electrode, the as-prepared active materials were mixed and ground with Super P conductive carbon (TIMCAL Graphite & Carbon), and

poly(vinylidene difluoride) (PVDF, Sigma-Aldrich) binder dispersed in an N-methyl-2-pyrrolidone (NMP, Alfa Aesar) solution at a weight ratio of 80:10:10, respectively. The as-prepared slurry was uniformly spread and pressed onto Cu foil and dried in a vacuum oven at 80 °C overnight as the working electrode. CR2016-type coin cells were assembled in an argon-filled glovebox (Innovative Technology, IL-2GB) with the working electrodes, pure lithium foil as the counter electrodes, and polypropylene film as the separator. 1 M $LiPF_6$ in the mixture of ethylene carbon (EC)/dimethyl carbonate (DMC) (volume ratio of 1:1, with 2% vinylene carbonate (VC) as the additive) was used as the electrolyte. All electrochemical measurements were performed with the assembled two-electrode battery at ambient temperature.

Galvanostatic discharge and charge measurements were performed with LAND CT2001A tester (Wuhan, China) at different current densities in the voltage range of 0.01-3.5 V versus Li^+/Li. Cyclic voltammetry (CV) was conducted on an electrochemical analyzer (CH Instruments, model 605C) in the voltage range of 0.01-3.0 V (vs. Li/Li^+) at a scan rate of 0.1 mV s^{-1}. Alternating current (AC) impedance was recorded on the electrochemical analyzer (CH Instruments, model 605C) with amplitude of 5.0 mV in the frequency range from 100 kHz to 0.01 Hz. The half-cells were tested at various current rates based on the weight of the active material alone.

3. Results and discussion

XRD pattern of C-mcms shown in Fig.3 demonstrates no distinct diffraction peaks, suggesting the amorphous feature of the SiO_2. A broad and weak diffraction peak located in the 2θ range of 21-23° should be associated with amorphous SiO_2. Fig. 4 shows the high-resolution XPS spectra of C_{1s} and Si_{2p} for sample mcms and C-mcms. The binding energy scales of the spectra were calibrated by assigning the most intense C_{1s} peak a binding energy of 285.2 eV. As shown in Fig. 4a, compared with mcms, the intensity of O-C=O (289.2 eV) peak decreases, and another peak at 289.7 eV related to the asymmetric shape of non-graphic carbon[32] appears when coated with carbon outside the SiO_2. However, it is clearly indicated that there is only one peak at 104.4 eV ascribed to Si^{4+} can be found in the carbon coated mcms, as shown in Fig. 3b, suggests the single amorphous phase of SiO_2 [33, 34], which demonstrates SiO_2 was not reduced to other forms of Si-O composites.

TGA was used to determine the SiO_2 content in the C-mcms, C-ms and mcms composites, as shown in Fig. 5, the SiO_2 content reached 73.5%, 83.4% and 87%, respectively.

Fig. 6 presents the general view of the morphologies of mcms, C-mcms, ms, and C-ms. Among them, mcms exhibits a relatively uniform shape without agglomeration (Fig. 6a), and this structure retains after carbon coating on the surface (C-mcms, Fig. 6b). Comparatively, when mcms was converted to ms after calcination in air for 3 h, some of the mesoporous silica (ms) spheres collapsed and broke into fragments due to the gas escape, the uniform shape was also destroyed, as shown in Fig. 6c. Even coated with a layer of carbon, the same disordered morphology retained(C-ms, Fig. 6d), which may result in a high surface area and surface energy. Lower magnification SEM images of these samples are shown in Fig.S1, the general view of the morphology of these three samples are in consistence with above description.

Nitrogen adsorption measurement was used to determine the pore structure of the mcms, C-mcms, ms and C-ms composites. Fig. 7 gives their adsorption-desorption and the pore size distribution curve. All four samples exhibit type IV isotherms with a typical H4 type hysteresis loop, which is nearly parallel over an appreciable range of relative pressure, according to IUPAC classification. The open H4 type hysteresis loop can be attributed to the mesoporous structures formed by slit-like pores and the aggregation of particles, internal voids in the spheres [35]. The core-shell structured mcms nanospheres sample shows a relatively narrow pore size distribution from 1.5-3 nm, indicating the existence of mesopores originated from the mesoporous silica shell and mesoporous carbon core. During the carbon coating process, some of the sucrose molecules (with molecular diameter about 0.9 nm) were absorbed into these nanopores, and blocked them during carbonization, which resulted in the significant decrease of the detected specific surface area and pore volume. Similar phenomenon also happens for C-ms sample. The surface areas of the core-shell mcms, C-mcms and C-ms are calculated to be 1226, 273 and 506 $m^2 \cdot g^{-1}$, respectively. The corresponding pore volume are also calculated to be 0.30, 0.17 and 0.19 $cm^3 \cdot g^{-1}$, in which C-mcms demonstrates the lowest surface area and pore volume. The specific surface area and pore volume of the four samples are listed in Table. 1.

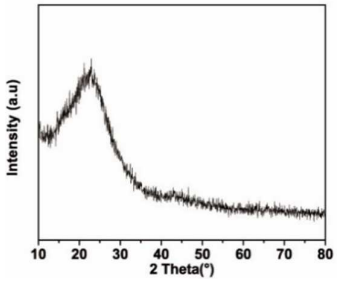

Fig. 3 XRD pattern of the C-mcms composite.

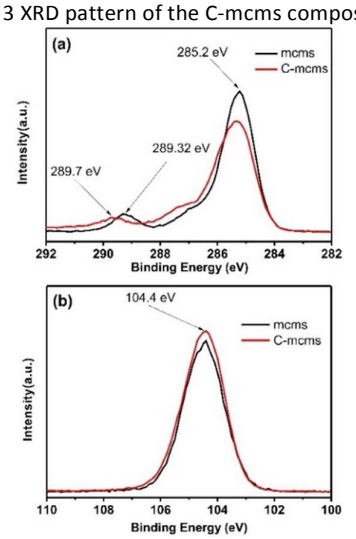

Fig. 4 High-resolution XPS spectra of C_{1s} (a) (inset: enlarge part of the C_{1s} spectra) and Si_{2p} (b) for C-mcms and mcms composites.

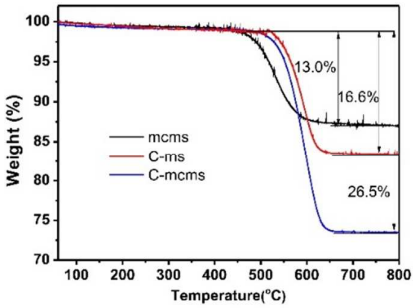

Fig.5 The TGA curves of the C-mcms, C-ms and mcms composites from 25 ℃ to 800 ℃ at a heating rate of 10 ℃·min^{-1} in a flow air.

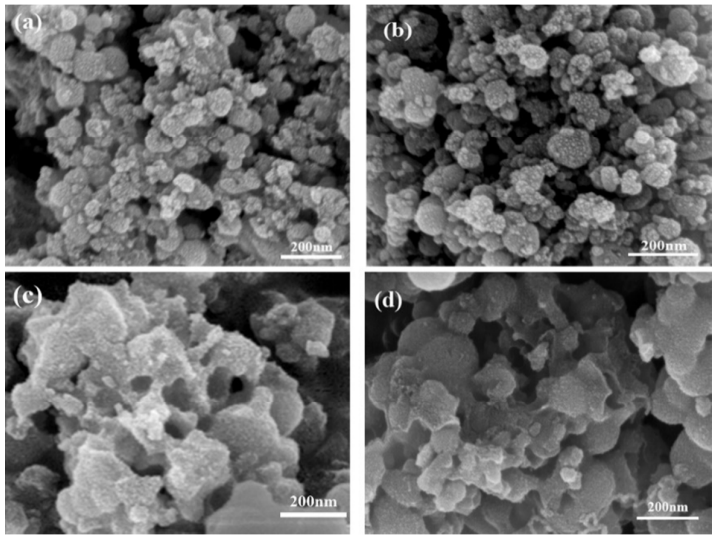

Fig. 6 SEM images of the carbon core-mesoporous silica without carbon shell(mcms) (a), carbon core-mesoporous silica-carbon shell(C-mcms) (b), hollow mesoporous silica nanospheres without carbon shell and carbon core(ms)(c), and hollow mesoporous silica nanospheres -carbon shell without carbon core(C-ms) (d).

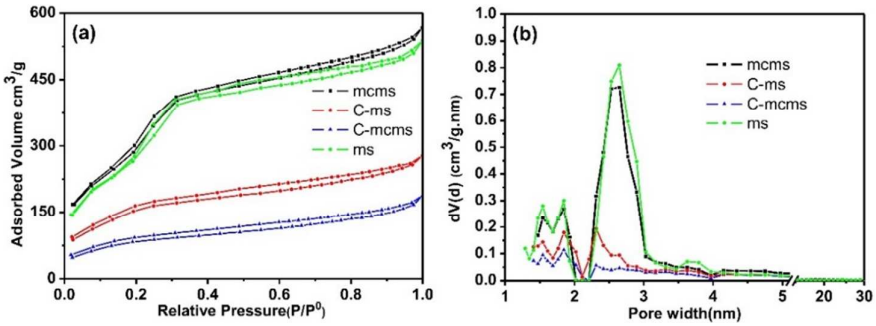

Fig. 7 Nitrogen adsorption-desorption isotherms (a) and the Density Functional Theory (DFT) pore size distribution (b) of mcms, C-mcms, ms and C-ms.

Table. 1. The specific surface area and pore volume of the as prepared C-mcms, C-ms, mcms, and ms

Sample	Bet surface area($m^2 \cdot g^{-1}$)	Pore volume ($cm^3 \cdot g^{-1}$)
C-mcms	273	0.17
C-ms	506	0.19
mcms	1226	0.30
ms	1188	0.27

As the density of SiO_2 is 2.65 g·cm^{-3}, the average particle size of SiO_2 (d) can be calculated based on the Nitrogen-adsorption derived surface area.

$S=\pi d^2$

$V=\pi d^3/6$

$Sw = S/\rho V = 6/\rho d$

d=6/ρSw=6/(2.65*106*1188.0)=1.90 nm

Transmission electron microscopy (TEM) was also carried out to provide further insight into the morphology and structure of the resulting C-mcms composites. As shown in Fig. 8, the carbon sphere core, porous silica layer, and carbon shell are organized compactly, which is in good accordance with the designed three layer structure. The size of each part of the C-mcms particle from inside to outside can also be measured to be about 100 nm diameter for the carbon core (the lighter area inside), 50 nm thick for the mesoporous silica layer (the darker area) and about 6 nm thick for the carbon shell (the lighter layer outside, and the carbon layer of the C-mcms was also observed by HRTEM, and shown in Fig. 8c). It can be clearly found that the whole C-mcms spheres demonstrate a uniform size of 200 ± 10 nm, and are also dispersed well without agglomeration. STEM linescan was also carried out in order to further demonstrate the carbon-silica-carbon three layer structure of C-mcms. The Si, O, C element distribution with the depth of the scanning point is shown in Fig.8d. As we can see, there are no Si, O, C elements detected at the start point. C element shows a high content at the two edges of the scan line and the middle part of the particle, which refers to the carbon layer and carbon core, respectively. Correspondingly, Si and O element show a higher content between the carbon layer and the carbon core, which refers to the SiO_2 layer. Moreover, the Si and O element content decreases in the middle of the particle, with the increase of carbon content, which also confirms the three layer structure of C-mcms. TEM images of mcms and C-ms are also shown in Fig. S2, the mcms spheres demonstrate a uniform morphology and are also dispersed well without agglomeration (Fig. S2a), which is similar with the C-mcms. However, the uniform structure collapsed and broke into fragments after calcination, some parts of the C-ms particles also cannot be covered by carbon layer, as shown in Fig. S2b, which is in consistence with the description of SEM images.

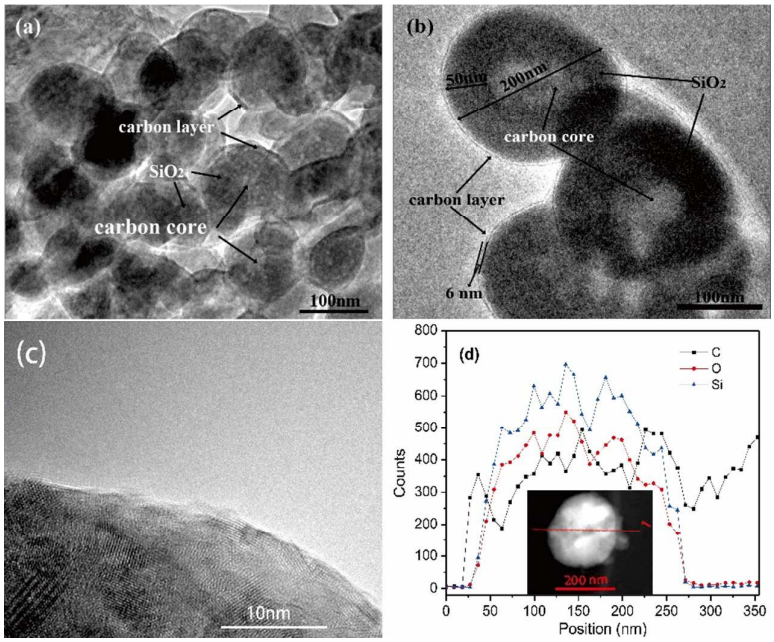

Fig. 8 TEM images of the C-mcms (a), (b), HRTEM of the carbon layer (c), and STEM linescan of the three layer structure of C-mcms (d).

The electrochemical performance of the synthesized C/SiO_2 composites as anode materials for lithium ion batteries was evaluated using CR2016 coin-type half-cells in the voltage range of 0-3.5 V.

The cyclic voltammetry (CV) curves of C-mcms at a scanning rate of 0.1 mV·s^{-1} were displayed in Fig. 9. Several obviously reduction peaks located at 1.45V, 1.26V and 0.70V can only be found in the first cycle. The small peaks at 1.45 V and 1.26 V may be attributed to side reactions between electrolyte and electrode and the beginning formation of the solid electrolyte interface (SEI) layer on the electrode surface. The peak at 1.26V may result from the reductive decomposition of vinylene carbonate (VC) as the additive in the electrolyte[36]. According to the literature, the reduction peaks at around 1.0-1.5 V may be associated with the side reaction of Li^+ with the residual oxygen-containing groups in the carbon shell or carbon core, which also consumes lithium ions and results in irreversible capacities[22]. But the specific reaction between electrolyte and electrode still remain unclear, more work may need to be done to explain it. While the long cathodic plateau at 0.70 V is associated with the electrolyte decomposition and the formation of SEI layer on the surface of the electrode[22, 30, 36]. As reported, the formation of the solid electrolyte interface (SEI) layer on the electrode surface may contribute a lot of the irreversible capacitance, and result in a low initial coulombic efficiency. And

from the second cycle, all these peaks would disappear. The long cathodic peak below 0.5V in the first cycle should be assigned to the electrochemical reduction of SiO_2 to Si, the irreversible formation of Li_2O or Li_4SiO_4 (eqn.1a, b), and the insertion of lithium into active materials, including Si and carbon [29, 36, 37]. These reactions can be summarized as follows:

$2SiO_2 + 4Li^+ + 4e^- \rightarrow Li_4SiO_4 + Si$ 1(a)

$SiO_2 + 4Li^+ + 4e^- \rightarrow 2Li_2O + Si$ 1(b)

$Si + xLi^+ + xe^- \leftrightarrow Li_xSi$ 2

$C + yLi^+ + ye^- \leftrightarrow Li_yC$ 3

Even though the inert Li_2O and Li_4SiO_4 generated by the reaction 1(a) and 1 (b) contribute the major irreversible capacity, however, together with carbon, they can also act as a matrix to support and disperse the nano-Si from aggregation and buffer the volume change during cycling, which is benefit to keep a stable cycling performance, evidenced by the following stable CV profiles after the first cycle. Both Si and carbon will alloy/dealloy with lithium reversibly and provides the reversible capacity (Reaction 2 and 3) in the following cycles.

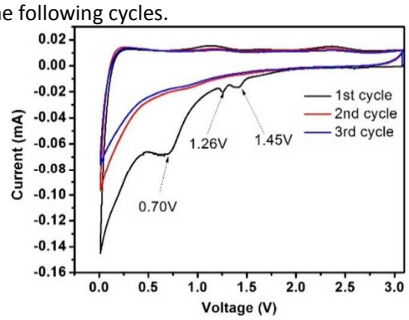

Fig. 9 Cyclic voltammetry profiles of the C-mcms electrode measured in the voltage range of 0.01-3.0 V (vs. Li/Li^+) with a scan rate of 0.1 $mV \cdot s^{-1}$.

Fig. 10 displays the charge-discharge profiles of the three C/SiO_2 composites for the initial three cycles in the voltage range of 0.01 to 3.5 V at a current density of 100 $mA \cdot g^{-1}$. Specifically, as shown in Fig. 10a, there are two small plateaus located at 1.45V and 1.26V and one relatively longer plateau located at 0.7V, these can only be found on the first discharge curve, which is in consistent with the peaks in CV profile. The initial discharge capacity of the C-mcms is found to be 2547 mA $h \cdot g^{-1}$, while the charge capacities reaches 1438 mA $h \cdot g^{-1}$, with an initial coulombic efficiency of 56.5%. By reducing the diameter of the SiO_2 particles into nanosize, it may make the reaction more readily to complete in the first several cycles compared with the large particle size. The coulombic efficiency rises to 96% in the 2nd cycle, and remains at approximately 100% in the following cycles. The high coulombic efficiency indicates a stable SEI film on the electrode surface. The coulombic efficiency climbing to above 90% in the second cycle is common in SiO_2 [38, 39] and other anode materials, for example, the CE of Si/H-rGO composite film rise from 47% in the first coulombic efficiency to above 94% in the subsequent cycles [40]. By reducing the diameter of the SiO_2 particles into nanosize, it may make the reaction more easily to complete compared with the large particle size. However, the first charge capacity of C-ms and mcms only reaches 516 and 123 $mAh \cdot g^{-1}$, and the corresponding coulombic efficiency are calculated to be 33.8% and 18.6%, respectively. Both charge capacity and coulombic efficiency of C-mcms are much larger than C-ms and mcms. According to previous reports [22, 30, 41, 42], the irreversible capacity loss in the first cycle is mainly ascribed to the formation of the solid electrolyte interphase and electrolyte degradation.

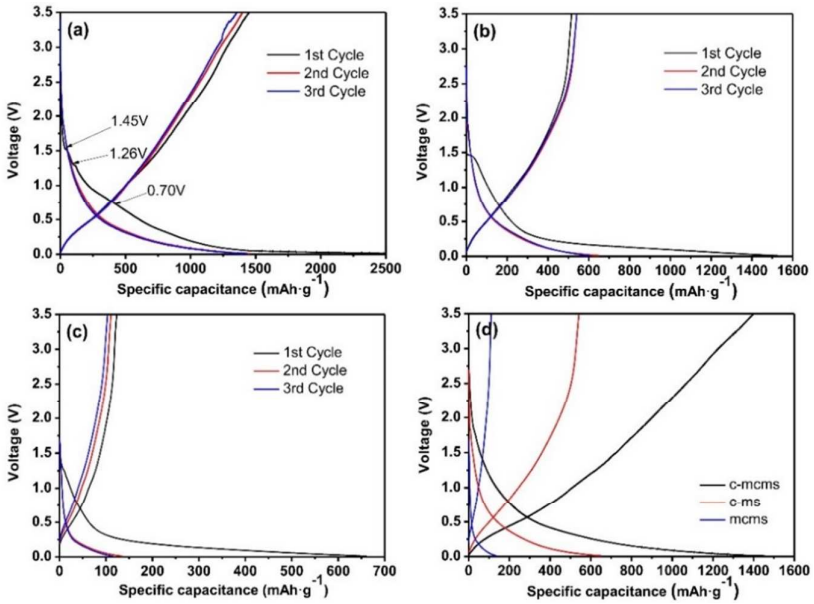

Fig. 10 First three discharge and charge curves of the C-mcms(a), C-ms (b) and mcms (c) electrode at a current density of 100 $mA \cdot g^{-1}$ and the comparison of 2nd discharge and charge curves of the three samples (d).

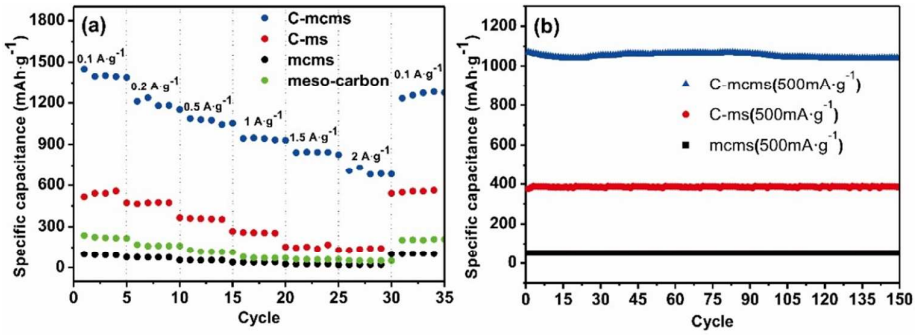

Fig. 11 (a) The comparison of the rate capability of the three samples and mesoporous carbon at different current densities and (b) The comparison of the cycling performance of the three samples at a current density of 500 mA·g^{-1}.

The rate performance of the three synthesized C/SiO_2 composites at various charge-discharge rates were also evaluated and compared. As shown in Fig. 11a, C-mcms was found to demonstrate a better rate performance compared to C-ms and mcms at each current density. For example, it demonstrates little difference in charge capacity between different current densities and presents a higher reversible capacity of approximately 1400 mAh·g^{-1} at a current density of 100 mA·g^{-1} and nearly 660 mAh·g^{-1} even at a current density of 2000 mA·g^{-1}, demonstrating the excellent high rate performance for high power lithium-ion battery. More significantly, the C-mcms electrode also displays a good capacity recovery when the current density switches back from 2000 mA·g^{-1} to 100 mA·g^{-1}, suggesting good electrode structure stability. However, the other two electrodes, C-ms and mcms deliver much lower capacities at different testing current densities, for example, C-ms delivers only 605 mAh·g^{-1} and mcms delivers only a capacity of 110 mAh·g^{-1} at a current density of 100 mA·g^{-1}. The rate performance of mesoporous silica was also studied and shown in Fig.S3, the capacity only reaches 115-120 mAhg^{-1} at a current density of 100 mA·g^{-1} due to its low conductivity, which is similar with that of mcms. The results demonstrate that without carbon coating on the surface of SiO_2 particles, the conductivity and capacity would be extremely low.

The cycle performance of the three different samples were also evaluated for 150 cycles at the current density of 500mA·g^{-1}, as shown in Fig. 11b, C-mcms electrode delivers the highest reversible specific capacitance of more than 1055 mAh·g^{-1}, and can be maintained for 150 cycles without any tendency of degradation. According to the TGA result of C-mcms, considering the 26.5 % percent of carbon (with the specific capacitance to be 130 mAh·g^{-1}, shown in Fig. 11a), it can be calculated that the specific charge capacity of silica component is about 1388 mAh·g^{-1}. However, the C-ms and mcms can only deliver a capacitance of 385 mAh·g^{-1} and 55 mAh·g^{-1} at a current density of 500 mA·g^{-1}, respectively. The three samples can all demonstrate a stable cycling performance, which suggests that a stable matrix was formed to support and disperse the nano-Si from aggregation and buffer the volume change during cycling.

Due to the absence of carbon coating on the surface of mesoporous silica, the conductivity of mcms could be very poor, it becomes relatively more difficult for the transportation of lithium ion throughout the silica particles, thus demonstrating a very low initial discharge capacity. Moreover, the high specific area of mcms indicates the SiO_2 are exposed to the electrolyte directly, results in increasing more side reactions with the electrolyte to form excessive SEI layer on the surface of SiO_2 particles and causing the loss of electrical connection to the active material, thus leading to the poor coulombic efficiency and a big capacity decay, which is almost 80% of the first discharge capacity loss. For the C-ms with a carbon layer coated on the surface of hollow mesoporous silica spheres, rate and cycle performance are improved to a great extent compared with the mcms. The conductive carbon framework can restrain the volume change of silica and guarantee rapid electron transfer throughout the composite. However, due to the structure collapse and deformation during calcination, some parts of the mesoporous SiO_2 particles cannot be covered or filled by carbon, which results in the high surface area and pore volume (Bet surface area: 506 $m^2 \cdot g^{-1}$, Pore volume: 0.19 $cm^3 \cdot g^{-1}$, respectively), and thus lowering the integral conductivity. The uncoated or unfilled parts of SiO_2 are still exposed to the electrolyte and it also results in the formation of excessive SEI layer and thus lowering the reversible capacity.

In contrast, the C-mcms with a three layer structure exhibits the best cycle performances. Fig. 12 shows the cycling performance with coulombic efficiency of C-mcms electrode at a high current density of 500 mA·g^{-1}. As we can see, C-mcms demonstrates an excellent charge-discharge reversibility and superior cycling stability, with a high reversible capacity of more than 1055 mAh·g^{-1} with the coulombic efficiency stays at nearly 100% during the cycles. The excellent electrochemical performance may mainly be ascribed to the refined structure design: Firstly, the three layer structure ensures the porous silica nanoparticles be completely confined between carbon core and the carbon shell, as shown in the TEM picture. The carbon core and carbon shell together act as a mechanical backbone to support the SiO_2 nanoparticles to be electrochemically active and help to keep the structural integrity during cycling; Secondly, after carbon coated on the surface of the mcms spheres and partly inside the silica nanopores, although just several nanometres thick, it not only acts as an electrical highway to reduce the transport distance of electron/lithium ions, but also lowers the surface area and results in less side reactions and less formation of SEI. The carbon coated on the surface of SiO_2 is also crucial for blocking the electrolyte outside of the whole particle, minimizing the direct exposure of SiO_2 particles to the electrolyte,

and limiting majority of SEI formation to the outer surface of the carbon rather than the excessively formation on the SiO_2 particles. Similar results have been reported before, by encapsulating nano silicon particles in a carbon chamber or hollow carbon spheres, the electrochemical performance can be greatly enhanced[11, 20, 21]. Thirdly, as the average particle size of SiO_2 is calculated to be only 1.90 nm, the ordered internal void space with an average diameter of 2.65 nm (from the PSD, Fig .7b) among these nanoparticles can provide free space to accommodate the mechanical strain and allow the Si to expand without pulverization during Li^+ intercalation and deintercalation process[11, 21, 43] and help to form a relatively stable mixture, as illustrated in Fig. 13, the SEI layer formed outside of the carbon shell is helpful for maintaining a stable charge capacity and high coulombic efficiency. The assumption can be further confirmed by the SEM investigation of the C-mcms before and after cycling, as shown in Fig. 14, C-mcms nanospheres composite electrode did not crack and pulverize after 150 charge/discharge cycles. Fourthly, the inert Li_2O and Li_4SiO_4 generated during the first lithiation process, together with the carbon layer, can also help to improve the cycle stability by buffering the big volume change caused by the lithiation of active Si. Besides, by tailoring SiO_2 particles into nanosize using surfactant template, together with the nanopores among the SiO_2 particles, the diffusion distance of lithium ion and electrons can be effectively reduced, thereby facilitating faster lithium ion transport in the silica matrix and ensuring an enhanced structural stability and cycle performance [22, 30]. At the same time, the local current density can also be decreased due to the high specific surface area of the silica nanoparticles [44].

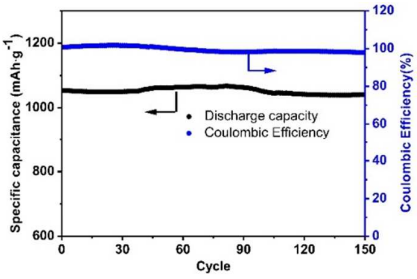

Fig. 12 Cycling performance of the C-mcms electrode at a current density of 500 mA·g^{-1}.

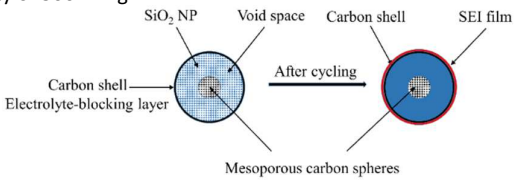

Fig. 13 Simplified two-dimensional cross-section view of one C-mcms sphere before and after electrochemical cycling.

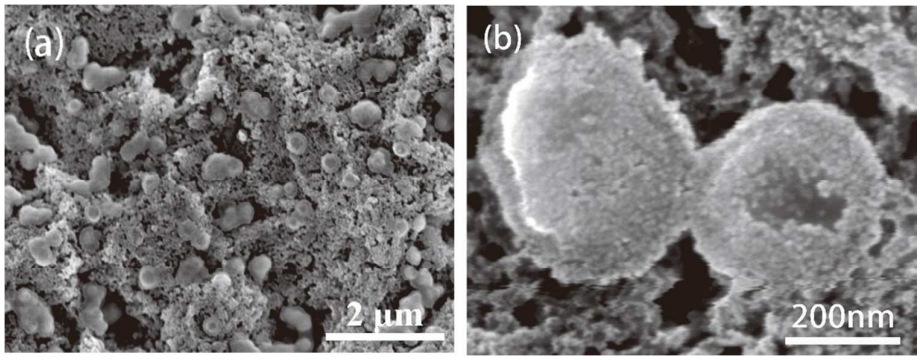

Fig. 14 SEM images of the C-mcms electrode after 150 cycles (a), (b)

To further investigate the influence of different structures on the electrochemical performance of the three C/SiO_2 electrodes for lithium-ion energy storage, EIS measurement was performed over a frequency range of 100 kHz to 0.01 Hz. Fig. 15a shows the Nyquist plots of the three electrodes after 30 cycles to ensure the formation of stable SEI films. The resistance R_{sf} ascribed to the surface film and the charge transfer resistance R_{ct} due to the electrode reaction in the electrode-electrolyte interface are combined in a depressed semicircle in the high frequency region[45]. The long slope line represents the Warburg impedance (Z_W) at low frequency region, which indicates the diffusion of lithium ions in the solid matrix. The equivalent electrical circuit model (as shown in inset Fig. 13a) was used to fit the three Nyquist plots, in which the symbols, R_s, R_f, R_{ct} and Z_W, represents the solution resistance, contact resistance, charge-transfer resistance and Warburg impedance, respectively. The fitting results are listed in Table 2. The R_f and R_{ct} values of C-mcms electrode are 103.6 Ω and 68.2 Ω, respectively, which are the lowest compared with the other two electrodes. These results suggest that the special three layer structure with carbon coating outside the mesoporous silica spheres lowers the contact and charge-transfer impedances, which is in consistence with above analysis. The lithium ion diffusion coefficient (D_{Li}) could be calculated from the low frequency plots based on the following equations:

$$Z' = R_e + R_{ct} + \sigma\omega^{-0.5} \quad (4)$$

$$D_{Li} = \frac{(RT)^2}{2(An^2F^2C_{Li}\sigma)^2} \quad (5)$$

In eqn 4, $\omega(2\pi f)$ is the angular frequency in the low frequency region, both $R_e + R_{ct}$ and Warburg coefficient (σ) can be obtained from the fitting line while Z' has a linear relationship with $\omega^{-0.5}$.

In eqn 5, T is the absolute temperature, R is the gas constant, A is the surface area of the electrode, n is the number of electrons transfer per mole of the active material involved in the electrode reaction, F is Faraday's constant, and C_{Li} is the molar concentration of lithium ions. Based on the fitting linear equation in Fig. 15b, the lithium ion diffusion coefficients of C-mcms, C-ms and mcms are calculated to be approximately 1.19×10^{-17} $cm^2 \cdot s^{-1}$, 5.07×10^{-18} and 4.79×10^{-19} $cm^2 \cdot s^{-1}$, respectively. The lowest surface film and charge transfer resistance and higher lithium ion diffusion coefficient and electrical conductivity confirm that C-mcms has a more conductive pathway for lithium-ions transportation than the other two electrodes, resulting in enhancement in the electrochemical properties.

Table 2. Impedance parameters calculated from equivalent circuit.

Sample	Rs(Ω)	Rf(Ω)	Rct(Ω)
mcms	8.3	240.2	507.3
C-ms	11.9	120.5	264.3
C-mcms	7.02	103.6	68.2

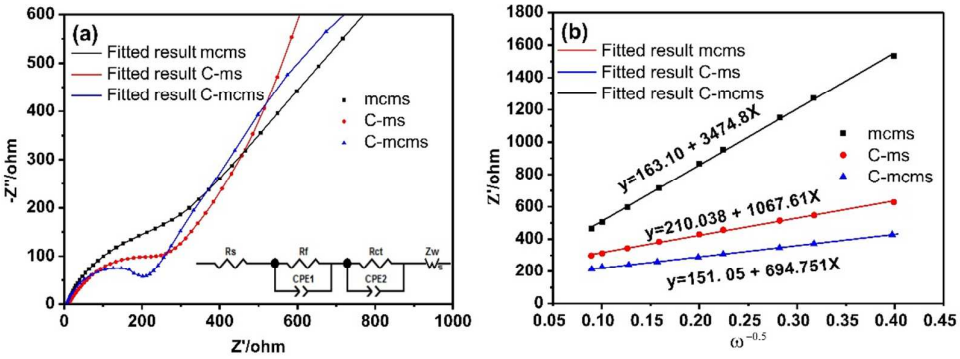

Fig. 15 (a) The EIS plots of the three samples at 25 ℃ (inset: equivalent electrical circuit model) and (b) the Z′-$\omega^{-0.5}$ plots in the low frequency range.

4. Conclusions

In summary, a new type of C/SiO_2 composite with a carbon-mesoporous silica-carbon three layer structure was synthesized and evaluated as an anode material for high-energy lithium-ion batteries. The as-prepared composite with such a refined structure exhibits an excellent electrochemical capacity and cycle performance, and the effects of structure were systematically investigated with the comparison of similar composites without the carbon core or the carbon shell. It is revealed that the carbon shell may increase the integral electrical conductivity, decrease the SEI formation amount, and increase the initial coulombic efficiency, while the carbon core may support all SiO_2 nanoparticles to be electrochemically active. Meanwhile, the mesopores in the SiO_2 provided the free space to accommodate the volume expansion and helped to keep a stable mixture during cycling. Therefore, with rational and optimal design of the C/SiO_2 composites, the C-mcms composite is able to demonstrate excellent reversible capacity, high rate capability and cyclic stability, and show great potential for application as the next generation of anode materials for high-energy lithium-ion batteries.

Acknowledgements

This work was supported by the National Natural Science Foundation of China (grant No.51274015) and National Science Foundation (NSF-DMR 1505902). Xi Cao and Shuang Li would also like to thank China Scholarship Council (CSC) for providing scholarship for their Ph.D. study at the University of Washington.

Reference

1. J. B. Goodenough and K. S. Park, *Journal of the American Chemical Society*, 2013, **135**, 1167-1176.
2. F. Cheng, J. Liang, Z. Tao and J. Chen, *Advanced Materials*, 2011, **23**, 1695-1715.
3. H. Li, Z. Wang, L. Chen and X. Huang, *Advanced Materials*, 2009, **21**, 4593-4607.
4. P. G. Bruce, B. Scrosati and J. M. Tarascon, *Angewandte Chemie - International Edition*, 2008, **47**, 2930-2946.
5. B. Dunn, H. Kamath and J. M. Tarascon, *Science*, 2011, **334**, 928-935.
6. Q. Zhang, E. Uchaker, S. L. Candelaria and G. Cao, *Chemical Society Reviews*, 2013, **42**, 3127-3171.
7. Y. Wang, H. Li, P. He, E. Hosono and H. Zhou, *Nanoscale*, 2010, **2**, 1294-1305.
8. P. Poizot, S. Laruelle, S. Grugeon, L. Dupont and J. M. Tarascon, *Nature*, 2000, **407**, 496-499.
9. W. W. Lee and J. M. Lee, *Journal of Materials Chemistry A*, 2014, **2**, 1589-1626.
10. V. Augustyn, J. Come, M. A. Lowe, J. W. Kim, P.-L. Taberna, S. H. Tolbert, H. D. Abruna, P. Simon and B. Dunn, *Nature Materials*, 2013, **12**, 518-522.

11. N. Liu, Z. Lu, J. Zhao, M. T. McDowell, H.-W. Lee, W. Zhao and Y. Cui, *Nat Nano*, 2014, **9**, 187-192.
12. C. Yu, X. Li, T. Ma, J. Rong, R. Zhang, J. Shaffer, Y. An, Q. Liu, B. Wei and H. Jiang, *Advanced Energy Materials*, 2012, **2**, 68-73.
13. H. Wu and Y. Cui, *Nano Today*, 2012, **7**, 414-429.
14. H. Wu, G. Chan, J. W. Choi, I. Ryu, Y. Yao, M. T. McDowell, S. W. Lee, A. Jackson, Y. Yang, L. Hu and Y. Cui, *Nature Nanotechnology*, 2012, **7**, 310-315.
15. H. Kim, M. Seo, M. H. Park and J. Cho, *Angewandte Chemie - International Edition*, 2010, **49**, 2146-2149.
16. H. Lin, W. Weng, J. Ren, L. Qiu, Z. Zhang, P. Chen, X. Chen, J. Deng, Y. Wang and H. Peng, *Advanced Materials*, 2014, **26**, 1217-1222.
17. K. Fu, Y. Lu, M. Dirican, C. Chen, M. Yanilmaz, Q. Shi, P. D. Bradford and X. Zhang, *Nanoscale*, 2014, **6**, 7489-7495.
18. J. Chang, X. Huang, G. Zhou, S. Cui, P. B. Hallac, J. Jiang, P. T. Hurley and J. Chen, *Advanced Materials*, 2014, **26**, 758-764.
19. R. Yi, F. Dai, M. L. Gordin, S. Chen and D. Wang, *Advanced Energy Materials*, 2013, **3**, 295-300.
20. B. Wang, X. Li, X. Zhang, B. Luo, Y. Zhang and L. Zhi, *Advanced Materials*, 2013, **25**, 3560-3565.
21. Y. Park, N. S. Choi, S. Park, S. H. Woo, S. Sim, B. Y. Jang, S. M. Oh, S. Park, J. Cho and K. T. Lee, *Advanced Energy Materials*, 2013, **3**, 206-212.
22. N. Yan, F. Wang, H. Zhong, Y. Li, Y. Wang, L. Hu and Q. W. Chen, *Scientific Reports*, 2013, **3**, 6.
23. W. S. Chang, C. M. Park, J. H. Kim, Y. U. Kim, G. Jeong and H. J. Sohn, *Energy & Environmental Science*, 2012, **5**, 6895-6899.
24. Q. Sun, B. Zhang and Z. W. Fu, *Appl. Surf. Sci.*, 2008, **254**, 3774-3779.
25. B. K. Guo, J. Shu, Z. X. Wang, H. Yang, L. H. Shi, Y. N. Liu and L. Q. Chen, *Electrochem Commun*, 2008, **10**, 1876-1878.
26. C. Ban, B. B. Kappes, Q. Xu, C. Engtrakul, C. V. Ciobanu, A. C. Dillon and Y. Zhao, *Applied Physics Letters*, 2012, **100**.
27. Y. Yao, J. J. Zhang, L. G. Xue, T. Huang and A. S. Yu, *Journal of Power Sources*, 2011, **196**, 10240-10243.
28. M. Sasidharan, D. Liu, N. Gunawardhana, M. Yoshio and K. Nakashima, *Journal of Materials Chemistry*, 2011, **21**, 13881-13888.
29. P. P. Lv, H. L. Zhao, J. Wang, X. Liu, T. H. Zhang and Q. Xia, *Journal of Power Sources*, 2013, **237**, 291-294.
30. Z. Favors, W. Wang, H. H. Bay, A. George, M. Ozkan and C. S. Ozkan, *Scientific Reports*, 2014, **4**, 7.
31. Y. Fang, G. Zheng, J. Yang, H. Tang, Y. Zhang, B. Kong, Y. Lv, C. Xu, A. M. Asiri, J. Zi, F. Zhang and D. Zhao, *Angewandte Chemie*, 2014, **126**, 5470-5474.
32. H. Estrade-Szwarckopf, *Carbon*, 2004, **42**, 1713-1721.
33. Y. Liu, T. P. Chen, Y. Q. Fu, M. S. Tse, J. H. Hsieh, P. F. Ho and Y. C. Liu, *Journal of Physics D: Applied Physics*, 2003, **36**, L97-L100.
34. S. Hofmann and J. H. Thomas Iii, *Journal of Vacuum Science and Technology B: Microelectronics and Nanometer Structures*, 1983, **1**, 43-47.
35. K. S. W. Sing, D. H. Everett, R. A. W. Haul, L. Moscou, R. A. Pierotti, J. Rouquerol and T. Siemieniewska, *Pure Appl. Chem.*, 1985, **57**, 603-619.
36. Y. J. Du, M. Y. Hou, D. D. Zhou, Y. G. Wang, C. X. Wang and Y. Y. Xia, *Journal of Energy Chemistry*, 2014, **23**, 315-323.
37. M. Q. Li, J. Li, K. Li, Y. Zhao, Y. G. Zhang, D. Gosselink and P. Chen, *Journal of Power Sources*, 2013, **240**, 659-666.
38. P. Lv, H. Zhao, C. Gao, T. Zhang and X. Liu, *Electrochim. Acta*, 2015, **152**, 345-351.
39. L. Zhang, J. W. Deng, L. F. Liu, W. P. Si, S. Oswald, L. X. Xi, M. Kundu, G. Z. Ma, T. Gemming, S. Baunack, F. Ding, C. L. Yan and O. G. Schmidt, *Advanced Materials*, 2014, **26**, 4527-+.
40. H. Tang, J. P. Tu, X. Y. Liu, Y. J. Zhang, S. Huang, W. Z. Li, X. L. Wang and C. D. Gu, *Journal of Materials Chemistry A*, 2014, **2**, 5834-5840.
41. X. Q. Yang, H. Huang, Z. H. Li, M. L. Zhong, G. Q. Zhang and D. C. Wu, *Carbon*, 2014, **77**, 275-280.
42. J. G. Tu, Y. Yuan, P. Zhan, H. D. Jiao, X. D. Wang, H. M. Zhu and S. Q. Jiao, *Journal of Physical Chemistry C*, 2014, **118**, 7357-7362.
43. H. Zhong, H. Zhan and Y. H. Zhou, *Journal of Power Sources*, 2014, **262**, 10-14.
44. P. Lv, H. Zhao, C. Gao, Z. Du, J. Wang and X. Liu, *Journal of Power Sources*, 2015, **274**, 542-550.
45. M. E. Orazem and B. Tribollet, *Electrochemical Impedance Spectroscopy*, 2011.

Graphical abstract:

Novel C/SiO_2 composite with a carbon-silica-carbon (C-mcms) three layer structure was synthesized and evaluated as an anode material for high-energy lithium ion batteries. The C-mcms exhibits excellent capacity of about 1055 $mAh \cdot g^{-1}$ at a current density of 500 $mA \cdot g^{-1}$ after 150 cycles without detectable decay, and high-rate capability, which is superior to other similar composites without the carbon core(c-ms) or the carbon shell (mcms).